NOTATION

c, concentration; λ, D, η, β, coefficients of thermal conductivity, diffusion, dynamic viscosity, and volume expansion; ρ, density; α, thermodiffusion constant; $\bar{T}$, mean temperature in operational gap; ΔT, temperature difference; $\varkappa = \sigma/H$; σ, column performance (extraction); $V(c_e, c_0)$, value function, see (16a); $q = c_e(1 - c_0)/c_0(1 - c_e)$; $H = \alpha g \rho^2 \beta \delta^3 (\Delta T)^2 B/6!\eta\bar{T}$, H*, see (4); $y_e = 504\alpha\eta DL/\rho g \beta \delta^4 \bar{T}$, y_e^*, see (4); δ, gap; L, column length; a, thermal diffusivity. Indices: 0, initial state; e, value near the refining end of column.

LITERATURE CITED

1. K. Cohen, The Theory of Isotope Separation, New York—Toronto—London (1961).
2. K. Aleksander, Usp. Fiz. Nauk, 74, No. 4, 711 (1962).
3. G. D. Rabinovich, R. Ya. Gurevich, and G. I. Bobrova, Thermodiffusion Separation of Liquid Mixtures [in Russian], Nauka i Tekhnika (1971).
4. K. Jones and V. Ferri, Isotope Separation by Thermodiffusion [Russian translation], IL, Moscow (1947).
5. J. W. Elder, J. Fluid Mech., 23, Part 1, 77 (1965).
6. P. J. Lloyd, Chem. Eng. Sci., 22, 1885 (1967).
7. P. L. Chueh and H. M. Yen, AIChE J., 13, No. 1, 37 (1967).
8. G. D. Rabinovich and R. Ya. Gurevich, Inzh.-Fiz. Zh., 22, No. 5, 825 (1972).

DYNAMICS OF PARTICLES IN A SPIRAL FLOW

V. I. Korobko, V. F. Grekov, and V. K. Shashmin

UDC 532.529

Dynamic characteristics have been derived for particles falling under gravity in a spiral heat-carrier flow.

Many theoretical studies have been made on the motion of small particles in turbulent flows, of which Chen's papers [1] form an important part.

Here we use Chen's equations [1] to determine the dynamic characteristics of a particle falling under gravity in a spiral flow within a rotating drying drum. The calculations are compared with experiment for particles falling in a homogeneous flow.

The equation of motion for a small spherical particle falling under gravity in a turbulent spiral gas flow within a rotating cylindrical drying drum takes the form

$$\frac{\pi}{6} d^3 \rho \vec{w} = \frac{\pi}{6} d^3 \rho \vec{g} + \frac{c_x}{2} \rho_1 \frac{\pi d^2}{4} |\vec{v}_1 - \vec{v}| (\vec{v}_1 - \vec{v}). \quad (1)$$

Equation (1) is derived from Chen's equation [1] by neglecting forces related to the acceleration of the fluid, as well as those due to the adjoint mass and the Basset force, which incorporates the history of the particle acceleration; this is done because these forces are small if the fluid is of low speed (3-7 m/sec) and the circumferential velocity is small ($v_\varphi = 1$ m/sec). Also, an assumption different from Chen's is that the viscous resistance is proportional to the square of the relative velocity $(\vec{v_1} - \vec{v})$ [2], with this force directed against the flow direction if the particle moves faster than the liquid, and vice versa.

We solve (1) for $\vec{w}$ on the basis that $c_x = 0.5$ [2], which gives

$$\vec{w} = \vec{g} + \frac{3}{8} \frac{\rho_1}{\rho} \frac{1}{d} |\vec{v}_1 - \vec{v}| (\vec{v}_1 - \vec{v}). \quad (2)$$

Chernyshevskii University, Saratov. Translated from Inzherno-Fizicheskii Zhurnal, Vol. 31, No. 2, pp. 264-269, August, 1976. Original article submitted May 21, 1975.

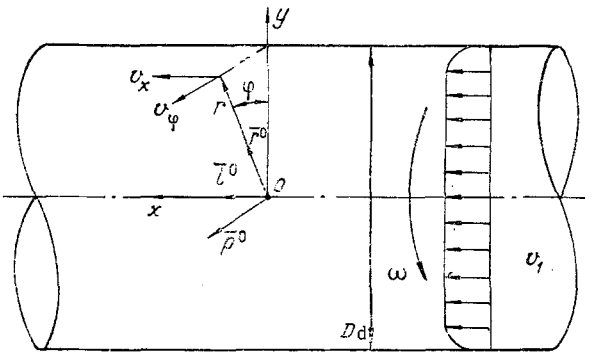

Fig. 1. Motion of particles within a rotating drum.

Equation (2) has been written in terms of projections on the axes of the cylindrical coordinate system (x, r, φ) (Fig. 1); we have used expressions for the projections of the acceleration and velocity vectors in terms of the radial component $\bar{r}^0$ and the transverse one $\bar{p}^0$ [3].

Let the drum rotate with angular velocity ω; the following velocity distribution is obtained for the fluid within the drum:

$$v_{1x} = v_1 = \text{const}, \quad v_{1r} = 0, \quad v_{1\varphi} = \omega r. \tag{3}$$

The following dimensionless quantities are now introduced:

$$\bar{x} = \frac{x}{D_d}, \quad \bar{r} = \frac{r}{D_d}, \quad \bar{\varphi} = \frac{\varphi}{2\pi}, \quad \bar{v}_x = \frac{v_x}{v_1}, \quad \bar{v}_r = \frac{v_r}{v_1},$$
$$\bar{v}_\varphi = \frac{v_\varphi}{\omega D_d}, \quad \bar{t} = \frac{v_1 t}{D_d}, \quad \bar{d} = \frac{d}{D_d}, \quad \bar{g} = g\frac{D_d}{v_1^2}. \tag{4}$$

Then (2) takes the following form in terms of projections on the directions $\bar{i}^0$, $\bar{r}^0$, and $\bar{p}^0$ (Fig. 1) on the basis of (3) and (4):

$$\frac{d\bar{v}_x}{d\bar{t}} = \frac{3}{8}\frac{\rho_1}{\rho}\frac{1}{\bar{d}}\sqrt{(1-\bar{v}_x)^2 + \bar{v}_r^2 + \frac{\omega^2 D_d^2}{v_1^2}(\bar{r}-\bar{v}_\varphi)^2}\,(1-\bar{v}_x),$$

$$\frac{d\bar{v}_r}{d\bar{t}} = -\frac{3}{8}\frac{\rho_1}{\rho}\frac{1}{\bar{d}}\sqrt{(1-\bar{v}_x)^2 + \bar{v}_r^2 + \frac{\omega^2 D_d^2}{v_1^2}(\bar{r}-\bar{v}_\varphi)^2}\,\bar{v}_r + \frac{\omega^2 D_d^2}{v_1^2}\frac{\bar{v}_\varphi^2}{\bar{r}} - \bar{g}\cos(2\pi\bar{\varphi}),$$

$$\frac{d\bar{v}_\varphi}{d\bar{t}} = \frac{3}{8}\frac{\rho_1}{\rho}\frac{1}{\bar{d}}\sqrt{(1-\bar{v}_x)^2 + \bar{v}_r^2 + \frac{\omega^2 D_d^2}{v_1^2}(\bar{r}-\bar{v}_\varphi)^2}\,(\bar{r}-\bar{v}_\varphi) - \frac{\bar{v}_r\bar{v}_\varphi}{\bar{r}} + \frac{v_1}{\omega D_d}\bar{g}\sin(2\pi\bar{\varphi}), \quad \frac{d\bar{x}}{d\bar{t}} = \bar{v}_x,$$
$$\frac{d\bar{r}}{d\bar{t}} = \bar{v}_r, \quad \bar{r}\frac{d\bar{\varphi}}{d\bar{t}} = \frac{\omega D_d}{2\pi v_1}\bar{v}_\varphi. \tag{5}$$

The last three equations have been written in accordance with the definitions of the velocity components v_X, v_r, and v_φ; also, the initial conditions are as follows:

$$t = 0: \qquad \bar{x} = \bar{x}_0, \quad \bar{r} = \bar{r}_0, \quad \bar{\varphi} = \bar{\varphi}_0,$$
$$\bar{v}_x = \bar{v}_{x0}, \quad \bar{v}_r = \bar{v}_{r0}, \quad \bar{v}_\varphi = \bar{v}_{\varphi 0}. \tag{6}$$

The solution to (5) with the boundary conditions of (6) serves to define the position of the particle within the drum in the spiral fluid flow, together with the components of the particle velocity, the path traveled, and the time of fall. Time t is taken as the parameter.

The assumptions made in deriving (6) have been tested by calculating the characteristics of a particle falling under gravity in a uniform fluid flow, and the results have been compared with experiment. In that case, the equations of motion take the form

$$\frac{d\bar{x}}{d\bar{t}} = \bar{v}_x, \quad \frac{d\bar{r}}{d\bar{t}} = \bar{v}_r, \quad \frac{d\bar{v}_x}{d\bar{t}} = \frac{3}{8\bar{d}}\frac{\rho_1}{\rho}\sqrt{(1-\bar{v}_x)^2 + \bar{v}_r^2}\times$$

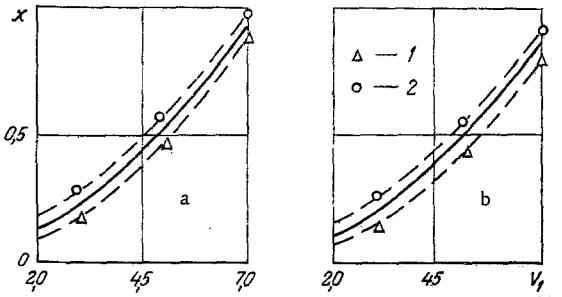

Fig. 2. Range of a particle of density ρ (kg/m^3) of 67.3 (a) and 72.9 (b) in terms of the speed v_1 (m/sec) for a homogeneous flow; the experimental values for the boundaries of the dispersal zone are as follows: a) x^e_{min}, the minimum range; 2) x^e_{max}, the maximum range. The solid lines have been derived by numerical solution of (7).

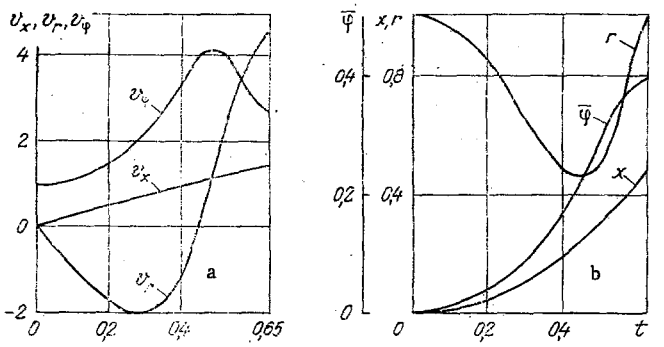

Fig. 3. Distributions of the dynamic parameters for a particle in a spiral flow (model No. 5) in relation to time t (sec): a) velocity distributions (axial v_X, radial v_r, and circumferential v_φ); b) distance moved x, distance from drum axis r, and angle of rotation φ around the x axis, rad/2π.

$$\times (1-\bar{v}_x), \quad \frac{d\bar{v}_r}{d\bar{t}} = -\frac{3}{8\bar{d}}\frac{\rho_1}{\rho}\sqrt{(1-\bar{v}_x)^2+\bar{v}_r^2}\,\bar{v}_r. \tag{7}$$

The initial conditions (for $\bar{t} = 0$) are as follows:

$$\bar{x} = \bar{\varphi} = \bar{v}_x = \bar{v}_r = 0, \quad \bar{r} = 1. \tag{8}$$

An M-220 computer was used to integrate (7) with the initial conditions of (8) by the Runge — Kutta method to the fourth order of accuracy [4]; the time step in the integration was H = 0.005 sec. We perform calculations on 10 different models for a constant density $\rho_1 = 1.225$ kg/m^3 for the fluid, two particle densities ρ of 67.3 and 72.9 kg/m^3, and five fluid speeds of v_1 = 3, 4, 5, 6, 7 m/sec. The diameter of a particle in all cases was d = 3 mm.

Figure 2a and b shows the calculated results for the projection of the distance traveled on the x axis, i.e., the range traveled, in relation to the speed v_1 of the fluid and the particle density ρ.

Measurements were made on the distances traveled by the particle in relation to flow speed; we used sunflower seeds of effective diameter d = 3 mm [5] and densities ρ of 67.3 and 72.9 kg/m^3. The working part of the wind tunnel had a horizontal surface at the lower part of the injection nozzle, which was parallel to the axis and which was covered with a layer of grease of thickness 3 mm, which served to define the points of incidence of the particles. The upper part of the nozzle had a device for supplying the seeds, and when the seeds emerged from this they fell under gravity in the working part of the tube onto the above plane. We used v_1 of 3, 5, and 7 m/sec. In each case we measured the distances traveled for 100 seeds, the range of distances

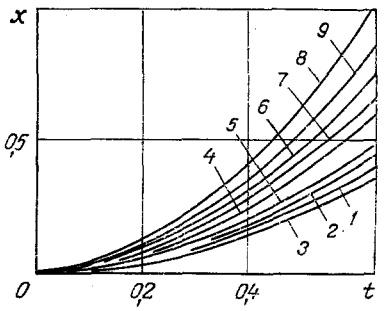

Fig. 4. Particle range x in relation to physical properties, fluid speed (the numbers are those of the models from Table 1), and time t.

TABLE 1. Physical Properties of Particles

Model number	Axial velocity v_1, m/sec	Fluid density ρ_1, kg/m³	Fluid temperature, °C	Density ρ of particles, kg/m³
1	4	9,45	200	72,9
2	4	9,45	200	67,3
3	4	6,14	300	72,9
4	5	9,45	200	72,9
5	5	6,14	300	72,9
6	6	9,45	200	72,9
7	6	6,14	300	72,9
8	7	9,45	200	72,9
9	7	6,14	300	72,9

being specified as the maximum value x^e_{max} and the minimum value x^e_{min}. The diameter of the nozzle was $D_d = 1$ m. Figure 2a and b shows the results, which agree satisfactorily with calculations from (7).

Consequently, (7) correctly reflects the behavior of particles in a uniform flow.

The assumptions involved in deriving (5) are the same as those for (7), but (5) is more general than (7), since it describes the motion in three-dimensional space, where (5) and (6) also correctly reflect the motion in a spiral flow.

We integrated (5) numerically by the Runge — Kutta method with an M-220 computer for the following cases subject to the initial condition t = 0:

$$\bar{x} = 0, \quad \bar{r} = 1, \quad \bar{\varphi} = 0, \quad \bar{v}_x = \bar{v}_r = 0, \quad \bar{v}_\varphi = 1. \tag{9}$$

The diameter of a spherical particle was d = 3 mm; the drum diameter $D_d = 2$ m, and the speed of rotation n = 9 rpm. Table 1 gives the numbers of the models and the various characteristics.

Figure 3a and b shows the results for model No. 5 in terms of the axial velocity v_x, radial velocity v_r, and circumferential velocity v_φ in relation to time t (Fig. 3a), and also the distance traveled x, the distance r from the axis of the drum, and the angle of circumferential displacement φ(rad/2π) in each case around the x axis, in relation to time t (Fig. 3).

Figure 4 shows the distance traveled as a function of time t, the physical parameters of the fluid ρ_1, the axial velocity v_1, and the particle density ρ. It is clear that for a constant fluid speed and fluid density (cases 1 and 2) the range increases as the particle density falls. At a constant speed and constant particle density, the range increases as the temperature falls (models 1 and 3). Analogous conclusions follow from the results for the other models. If the fluid speed is increased while all the physical parameters of the particles and fluid otherwise remain unchanged, the range increases, which corresponds to the physical picture of the behavior of a particle in response to a spiral flow and gravity.

NOTATION

d, sphere diameter; ρ, particle density; $\vec{v}$, particle velocity vector; $\vec{v}_1$, vector for mean velocity of heat carrier; $\vec{w}$, particle acceleration vector; $\vec{g}$, acceleration due to gravity; c_x, resistance coefficient for

a sphere; x, distance along the drum axis; r, distance from particle to drum axis; φ, angle between vertical axis and current radius-vector $\bar{r}$; $\bar{r}^0$, unit radius-vector in the $\bar{r}$ direction; $\bar{p}^0$, transverse direction; D_d, drum diameter; v_x, projection of particle velocity in x direction; v_r, radial velocity component; v_φ, angular velocity of particle; t, time; ω, angular velocity of drum.

LITERATURE CITED

1. J. O. Hinze, Turbulence: An Introduction to Its Mechanism and Theory, McGraw-Hill (1959).
2. L. G. Loitsyanskii, Mechanics of Liquids and Gases [in Russian], Nauka, Moscow (1970).
3. N. N. Bukhgol'ts, A Basic Textbook of Theoretical Mechanics [in Russian], Part 1, Nauka, Moscow (1969).
4. I. S. Berezin and N. P. Zhidkov, Computational Methods [in Russian], Vol. 2, Fizmatgiz, Moscow (1960).
5. V. A. Maslikov, Equipment for Producing Plant Oils [in Russian], Pishchevaya Promyshlennost', Moscow (1974).

PRESSURE DISTRIBUTION IN GAS FLOW IN THE PRESENCE OF A FIBROUS FILTER IN THE CHANNEL

B. I. Ogorodnikov, V. I. Skitovich, and V. I. Khabarov

UDC 536.24:532.526

The characteristics of gas flow through a fibrous filter in the presence of supercritical pressure drops are investigated.

Modern aerosol filters present porous systems of very long cylindrical fibers arranged in parallel planes randomly [1]. Their hydrodynamics, in particular of FP filters [2], has been well studied for relatively small velocities of the gas flows and small pressure drops at the filter [3-6]. For supercritical pressure drops when the ratio of static pressure behind the filter P_2 to the total pressure in front of the filter P_1 becomes smaller than 0.528 and the linear rates of filtration reach tens of meters per second, the gas flow in fibrous filters has not been investigated.

Isentropic gas flow in cylindrical channel [7] is known, which is a limiting case of gas flow through a filter whose resistance is equal to zero. The results of a computation of pressure distributions from the equation $P_1 = f(P_2, G)$ for different relative flow rates are given in Fig. 1 for the condition that the diameter of the channel is much larger than the mean free path of the gas molecules. Two characteristic zones can be separated out. In zone A, lying between straight lines I and II corresponding to equations $P_2 = 0.528P_1$ and $P_2 = P_1$, a decrease of P_2 for G = const results in a decrease of P_1. In zone B, lying between the straight line I and the ordinate, a change of P_2 for constant G does not effect P_1.

We introduce a quantity χ that is equal to the ratio of P_1 at any point on the curve $P_1 = f(P_2, G = \text{const})$ to the critical pressure P_1* at the intersection of this curve with line 1. Then zone A would be characterized by the values $\chi > 1$ while in zone B, $\chi = 1$.

Gas flow in multipath channels, i.e., labyrinths which are used, for example, in tube-machine construction [8], is also known. If the number of stages in the labyrinth is large, then in spite of the supercritical pressure drop between the input and the output of the labyrinth, the critical pressure drop at the last stage may not be reached. As seen from Fig. 1, the flow in the labyrinth differs substantially from the flow in a cylindrical channel discussed above; in zone B, χ is smaller than one. Thus, in spite of the supercritical pressure drop in the labyrinth as a whole, the decrease for P_2 for G = const leads to a decrease of P_1 everywhere.

Translated from Inzhenerno-Fizicheskii Zhurnal, Vol. 31, No. 2, pp. 270-273, August, 1976. Original article submitted June 26, 1975.